

Constraints on models for the Higgs boson with exotic spin and parity in $VH \rightarrow Vb\bar{b}$ final states

V.M. Abazov,³¹ B. Abbott,⁶⁷ B.S. Acharya,²⁵ M. Adams,⁴⁶ T. Adams,⁴⁴ J.P. Agnew,⁴¹ G.D. Alexeev,³¹ G. Alkhazov,³⁵ A. Alton^{a,56} A. Askew,⁴⁴ S. Atkins,⁵⁴ K. Augsten,⁷ C. Avila,⁵ F. Badaud,¹⁰ L. Bagby,⁴⁵ B. Baldin,⁴⁵ D.V. Bandurin,⁷³ S. Banerjee,²⁵ E. Barberis,⁵⁵ P. Baringer,⁵³ J.F. Bartlett,⁴⁵ U. Bassler,¹⁵ V. Bazterra,⁴⁶ A. Bean,⁵³ M. Begalli,² L. Bellantoni,⁴⁵ S.B. Beri,²³ G. Bernardi,¹⁴ R. Bernhard,¹⁹ I. Bertram,³⁹ M. Besançon,¹⁵ R. Beuselinck,⁴⁰ P.C. Bhat,⁴⁵ S. Bhatia,⁵⁸ V. Bhatnagar,²³ G. Blazey,⁴⁷ S. Blessing,⁴⁴ K. Bloom,⁵⁹ A. Boehnlein,⁴⁵ D. Boline,⁶⁴ E.E. Boos,³³ G. Borissov,³⁹ M. Borysova^{l,38} A. Brandt,⁷⁰ O. Brandt,²⁰ R. Brock,⁵⁷ A. Bross,⁴⁵ D. Brown,¹⁴ X.B. Bu,⁴⁵ M. Buehler,⁴⁵ V. Buescher,²¹ V. Bunichev,³³ S. Burdin^{b,39} C.P. Buszello,³⁷ E. Camacho-Pérez,²⁸ B.C.K. Casey,⁴⁵ H. Castilla-Valdez,²⁸ S. Caughron,⁵⁷ S. Chakrabarti,⁶⁴ K.M. Chan,⁵¹ A. Chandra,⁷² E. Chapon,¹⁵ G. Chen,⁵³ S.W. Cho,²⁷ S. Choi,²⁷ B. Choudhary,²⁴ S. Cihangir,⁴⁵ D. Claes,⁵⁹ J. Clutter,⁵³ M. Cooke^{k,45} W.E. Cooper,⁴⁵ M. Corcoran,⁷² F. Couderc,¹⁵ M.-C. Cousinou,¹² D. Cutts,⁶⁹ A. Das,⁴² G. Davies,⁴⁰ S.J. de Jong,^{29,30} E. De La Cruz-Burelo,²⁸ F. Déliot,¹⁵ R. Demina,⁶³ D. Denisov,⁴⁵ S.P. Denisov,³⁴ S. Desai,⁴⁵ C. Deterre^{c,20} K. DeVaughan,⁵⁹ H.T. Diehl,⁴⁵ M. Diesburg,⁴⁵ P.F. Ding,⁴¹ A. Dominguez,⁵⁹ A. Dubey,²⁴ L.V. Dudko,³³ A. Duperrin,¹² S. Dutt,²³ M. Eads,⁴⁷ D. Edmunds,⁵⁷ J. Ellison,⁴³ V.D. Elvira,⁴⁵ Y. Enari,¹⁴ H. Evans,⁴⁹ V.N. Evdokimov,³⁴ A. Fauré,¹⁵ L. Feng,⁴⁷ T. Ferbel,⁶³ F. Fiedler,²¹ F. Filthaut,^{29,30} W. Fisher,⁵⁷ H.E. Fisk,⁴⁵ M. Fortner,⁴⁷ H. Fox,³⁹ S. Fuess,⁴⁵ P.H. Garbincius,⁴⁵ A. Garcia-Bellido,⁶³ J.A. García-González,²⁸ V. Gavrilov,³² W. Geng,^{12,57} C.E. Gerber,⁴⁶ Y. Gershtein,⁶⁰ G. Ginther,^{45,63} O. Gogota,³⁸ G. Golovanov,³¹ P.D. Grannis,⁶⁴ S. Greder,¹⁶ H. Greenlee,⁴⁵ G. Grenier,¹⁷ Ph. Gris,¹⁰ J.-F. Grivaz,¹³ A. Grohsjean^{c,15} S. Grünendahl,⁴⁵ M.W. Grünewald,²⁶ T. Guillemain,¹³ G. Gutierrez,⁴⁵ P. Gutierrez,⁶⁷ J. Haley,⁶⁸ L. Han,⁴ K. Harder,⁴¹ A. Harel,⁶³ J.M. Hauptman,⁵² J. Hays,⁴⁰ T. Head,⁴¹ T. Hebbeker,¹⁸ D. Hedin,⁴⁷ H. Hegab,⁶⁸ A.P. Heinson,⁴³ U. Heintz,⁶⁹ C. Hensel,¹ I. Heredia-De La Cruz^{d,28} K. Herner,⁴⁵ G. Hesketh^{f,41} M.D. Hildreth,⁵¹ R. Hirosky,⁷³ T. Hoang,⁴⁴ J.D. Hobbs,⁶⁴ B. Hoeneisen,⁹ J. Hogan,⁷² M. Hohlfeld,²¹ J.L. Holzbauer,⁵⁸ I. Howley,⁷⁰ Z. Hubacek,^{7,15} V. Hynek,⁷ I. Iashvili,⁶² Y. Ilchenko,⁷¹ R. Illingworth,⁴⁵ A.S. Ito,⁴⁵ S. Jabeen^{m,45} M. Jaffré,¹³ A. Jayasinghe,⁶⁷ M.S. Jeong,²⁷ R. Jesik,⁴⁰ P. Jiang,⁴ K. Johns,⁴² E. Johnson,⁵⁷ M. Johnson,⁴⁵ A. Jonckheere,⁴⁵ P. Jonsson,⁴⁰ J. Joshi,⁴³ A.W. Jung,⁴⁵ A. Juste,³⁶ E. Kajfasz,¹² D. Karmanov,³³ I. Katsanos,⁵⁹ R. Kehoe,⁷¹ S. Kermiche,¹² N. Khalatyan,⁴⁵ A. Khanov,⁶⁸ A. Kharchilava,⁶² Y.N. Kharzheev,³¹ I. Kiselevich,³² J.M. Kohli,²³ A.V. Kozelov,³⁴ J. Kraus,⁵⁸ A. Kumar,⁶² A. Kupco,⁸ T. Kurča,¹⁷ V.A. Kuzmin,³³ S. Lammers,⁴⁹ P. Lebrun,¹⁷ H.S. Lee,²⁷ S.W. Lee,⁵² W.M. Lee,⁴⁵ X. Lei,⁴² J. Lellouch,¹⁴ D. Li,¹⁴ H. Li,⁷³ L. Li,⁴³ Q.Z. Li,⁴⁵ J.K. Lim,²⁷ D. Lincoln,⁴⁵ J. Linnemann,⁵⁷ V.V. Lipaev,³⁴ R. Lipton,⁴⁵ H. Liu,⁷¹ Y. Liu,⁴ A. Lobodenko,³⁵ M. Lokajicek,⁸ R. Lopes de Sa,⁶⁴ R. Luna-Garcia^{g,28} A.L. Lyon,⁴⁵ A.K.A. Maciel,¹ R. Madar,¹⁹ R. Magaña-Villalba,²⁸ S. Malik,⁵⁹ V.L. Malyshev,³¹ J. Mansour,²⁰ J. Martínez-Ortega,²⁸ R. McCarthy,⁶⁴ C.L. McGivern,⁴¹ M.M. Meijer,^{29,30} A. Melnitchouk,⁴⁵ D. Menezes,⁴⁷ P.G. Mercadante,³ M. Merkin,³³ A. Meyer,¹⁸ J. Meyer^{i,20} F. Miconi,¹⁶ N.K. Mondal,²⁵ M. Mulhearn,⁷³ E. Nagy,¹² M. Narain,⁶⁹ R. Nayyar,⁴² H.A. Neal,⁵⁶ J.P. Negret,⁵ P. Neustroev,³⁵ H.T. Nguyen,⁷³ T. Nunnemann,²² J. Orduna,⁷² N. Osman,¹² J. Osta,⁵¹ A. Pal,⁷⁰ N. Parashar,⁵⁰ V. Parihar,⁶⁹ S.K. Park,²⁷ R. Partridge^{e,69} N. Parua,⁴⁹ A. Patwa^{j,65} B. Penning,⁴⁵ M. Perfilov,³³ Y. Peters,⁴¹ K. Petridis,⁴¹ G. Petrillo,⁶³ P. Pétroff,¹³ M.-A. Pleier,⁶⁵ V.M. Podstavkov,⁴⁵ A.V. Popov,³⁴ M. Prewitt,⁷² D. Price,⁴¹ N. Prokopenko,³⁴ J. Qian,⁵⁶ A. Quadt,²⁰ B. Quinn,⁵⁸ P.N. Ratoff,³⁹ I. Razumov,³⁴ I. Ripp-Baudot,¹⁶ F. Rizatdinova,⁶⁸ M. Rominsky,⁴⁵ A. Ross,³⁹ C. Royon,¹⁵ P. Rubinov,⁴⁵ R. Ruchti,⁵¹ G. Sajot,¹¹ A. Sánchez-Hernández,²⁸ M.P. Sanders,²² A.S. Santos^{h,1} G. Savage,⁴⁵ M. Savitskyi,³⁸ L. Sawyer,⁵⁴ T. Scanlon,⁴⁰ R.D. Schamberger,⁶⁴ Y. Scheglov,³⁵ H. Schellman,⁴⁸ C. Schwanenberger,⁴¹ R. Schwienhorst,⁵⁷ J. Sekaric,⁵³ H. Severini,⁶⁷ E. Shabalina,²⁰ V. Shary,¹⁵ S. Shaw,⁵⁷ A.A. Shchukin,³⁴ V. Simak,⁷ P. Skubic,⁶⁷ P. Slatery,⁶³ D. Smirnov,⁵¹ G.R. Snow,⁵⁹ J. Snow,⁶⁶ S. Snyder,⁶⁵ S. Söldner-Rembold,⁴¹ L. Sonnenschein,¹⁸ K. Soustruznik,⁶ J. Stark,¹¹ D.A. Stoyanova,³⁴ M. Strauss,⁶⁷ L. Suter,⁴¹ P. Svoisky,⁶⁷ M. Titov,¹⁵ V.V. Tokmenin,³¹ Y.-T. Tsai,⁶³ D. Tsybychev,⁶⁴ B. Tuchming,¹⁵ C. Tully,⁶¹ L. Uvarov,³⁵ S. Uvarov,³⁵ S. Uzunyan,⁴⁷ R. Van Kooten,⁴⁹ W.M. van Leeuwen,²⁹ N. Varelas,⁴⁶ E.W. Varnes,⁴² I.A. Vasilyev,³⁴ A.Y. Verkheev,³¹ L.S. Vertogradov,³¹ M. Verocchi,⁴⁵ M. Vesterinen,⁴¹ D. Vilanova,¹⁵ P. Vokac,⁷ H.D. Wahl,⁴⁴ M.H.L.S. Wang,⁴⁵ J. Warchol,⁵¹ G. Watts,⁷⁴ M. Wayne,⁵¹ J. Weichert,²¹ L. Welty-Rieger,⁴⁸

M.R.J. Williams,⁴⁹ G.W. Wilson,⁵³ M. Wobisch,⁵⁴ D.R. Wood,⁵⁵ T.R. Wyatt,⁴¹ Y. Xie,⁴⁵ R. Yamada,⁴⁵ S. Yang,⁴ T. Yasuda,⁴⁵ Y.A. Yatsunenko,³¹ W. Ye,⁶⁴ Z. Ye,⁴⁵ H. Yin,⁴⁵ K. Yip,⁶⁵ S.W. Youn,⁴⁵ J.M. Yu,⁵⁶ J. Zennaro,⁶² T.G. Zhao,⁴¹ B. Zhou,⁵⁶ J. Zhu,⁵⁶ M. Zielinski,⁶³ D. Zieminska,⁴⁹ and L. Zivkovic¹⁴

(The D0 Collaboration*)

¹LAFEX, Centro Brasileiro de Pesquisas Físicas, Rio de Janeiro, Brazil

²Universidade do Estado do Rio de Janeiro, Rio de Janeiro, Brazil

³Universidade Federal do ABC, Santo André, Brazil

⁴University of Science and Technology of China, Hefei, People's Republic of China

⁵Universidad de los Andes, Bogotá, Colombia

⁶Charles University, Faculty of Mathematics and Physics,

Center for Particle Physics, Prague, Czech Republic

⁷Czech Technical University in Prague, Prague, Czech Republic

⁸Institute of Physics, Academy of Sciences of the Czech Republic, Prague, Czech Republic

⁹Universidad San Francisco de Quito, Quito, Ecuador

¹⁰LPC, Université Blaise Pascal, CNRS/IN2P3, Clermont, France

¹¹LPSC, Université Joseph Fourier Grenoble 1, CNRS/IN2P3,

Institut National Polytechnique de Grenoble, Grenoble, France

¹²CPPM, Aix-Marseille Université, CNRS/IN2P3, Marseille, France

¹³LAL, Université Paris-Sud, CNRS/IN2P3, Orsay, France

¹⁴LPNHE, Universités Paris VI and VII, CNRS/IN2P3, Paris, France

¹⁵CEA, Irfu, SPP, Saclay, France

¹⁶IPHC, Université de Strasbourg, CNRS/IN2P3, Strasbourg, France

¹⁷IPNL, Université Lyon 1, CNRS/IN2P3, Villeurbanne, France and Université de Lyon, Lyon, France

¹⁸III. Physikalisches Institut A, RWTH Aachen University, Aachen, Germany

¹⁹Physikalisches Institut, Universität Freiburg, Freiburg, Germany

²⁰II. Physikalisches Institut, Georg-August-Universität Göttingen, Göttingen, Germany

²¹Institut für Physik, Universität Mainz, Mainz, Germany

²²Ludwig-Maximilians-Universität München, München, Germany

²³Panjab University, Chandigarh, India

²⁴Delhi University, Delhi, India

²⁵Tata Institute of Fundamental Research, Mumbai, India

²⁶University College Dublin, Dublin, Ireland

²⁷Korea Detector Laboratory, Korea University, Seoul, Korea

²⁸CINVESTAV, Mexico City, Mexico

²⁹Nikhef, Science Park, Amsterdam, the Netherlands

³⁰Radboud University Nijmegen, Nijmegen, the Netherlands

³¹Joint Institute for Nuclear Research, Dubna, Russia

³²Institute for Theoretical and Experimental Physics, Moscow, Russia

³³Moscow State University, Moscow, Russia

³⁴Institute for High Energy Physics, Protvino, Russia

³⁵Petersburg Nuclear Physics Institute, St. Petersburg, Russia

³⁶Institució Catalana de Recerca i Estudis Avançats (ICREA) and Institut de Física d'Altes Energies (IFAE), Barcelona, Spain

³⁷Uppsala University, Uppsala, Sweden

³⁸Taras Shevchenko National University of Kyiv, Kiev, Ukraine

³⁹Lancaster University, Lancaster LA1 4YB, United Kingdom

⁴⁰Imperial College London, London SW7 2AZ, United Kingdom

⁴¹The University of Manchester, Manchester M13 9PL, United Kingdom

⁴²University of Arizona, Tucson, Arizona 85721, USA

⁴³University of California Riverside, Riverside, California 92521, USA

⁴⁴Florida State University, Tallahassee, Florida 32306, USA

⁴⁵Fermi National Accelerator Laboratory, Batavia, Illinois 60510, USA

⁴⁶University of Illinois at Chicago, Chicago, Illinois 60607, USA

⁴⁷Northern Illinois University, DeKalb, Illinois 60115, USA

⁴⁸Northwestern University, Evanston, Illinois 60208, USA

⁴⁹Indiana University, Bloomington, Indiana 47405, USA

⁵⁰Purdue University Calumet, Hammond, Indiana 46323, USA

⁵¹University of Notre Dame, Notre Dame, Indiana 46556, USA

⁵²Iowa State University, Ames, Iowa 50011, USA

⁵³University of Kansas, Lawrence, Kansas 66045, USA

⁵⁴Louisiana Tech University, Ruston, Louisiana 71272, USA

⁵⁵Northeastern University, Boston, Massachusetts 02115, USA

⁵⁶University of Michigan, Ann Arbor, Michigan 48109, USA

⁵⁷Michigan State University, East Lansing, Michigan 48824, USA

⁵⁸University of Mississippi, University, Mississippi 38677, USA

⁵⁹University of Nebraska, Lincoln, Nebraska 68588, USA

⁶⁰Rutgers University, Piscataway, New Jersey 08855, USA

⁶¹Princeton University, Princeton, New Jersey 08544, USA

⁶²State University of New York, Buffalo, New York 14260, USA

⁶³University of Rochester, Rochester, New York 14627, USA

⁶⁴State University of New York, Stony Brook, New York 11794, USA

⁶⁵Brookhaven National Laboratory, Upton, New York 11973, USA

⁶⁶Langston University, Langston, Oklahoma 73050, USA

⁶⁷University of Oklahoma, Norman, Oklahoma 73019, USA

⁶⁸Oklahoma State University, Stillwater, Oklahoma 74078, USA

⁶⁹Brown University, Providence, Rhode Island 02912, USA

⁷⁰University of Texas, Arlington, Texas 76019, USA

⁷¹Southern Methodist University, Dallas, Texas 75275, USA

⁷²Rice University, Houston, Texas 77005, USA

⁷³University of Virginia, Charlottesville, Virginia 22904, USA

⁷⁴University of Washington, Seattle, Washington 98195, USA

(Dated: August 28, 2014)

We present constraints on models containing non-standard model values for the spin J and parity P of the Higgs boson, H , in up to 9.7 fb^{-1} of $p\bar{p}$ collisions at $\sqrt{s} = 1.96 \text{ TeV}$ collected with the D0 detector at the Fermilab Tevatron Collider. These are the first studies of Higgs boson J^P with fermions in the final state. In the $ZH \rightarrow \ell\ell b\bar{b}$, $WH \rightarrow \ell\nu b\bar{b}$, and $ZH \rightarrow \nu\nu b\bar{b}$ final states, we compare the standard model (SM) Higgs boson prediction, $J^P = 0^+$, with two alternative hypotheses, $J^P = 0^-$ and $J^P = 2^+$. We use a likelihood ratio to quantify the degree to which our data are incompatible with non-SM J^P predictions for a range of possible production rates. Assuming that the production rate in the signal models considered is equal to the SM prediction, we reject the $J^P = 0^-$ and $J^P = 2^+$ hypotheses at the 97.6% CL and at the 99.0% CL, respectively. The expected exclusion sensitivity for a $J^P = 0^-$ ($J^P = 2^+$) state is at the 99.86% (99.94%) CL. Under the hypothesis that our data is the result of a combination of the SM-like Higgs boson and either a $J^P = 0^-$ or a $J^P = 2^+$ signal, we exclude a $J^P = 0^-$ fraction above 0.80 and a $J^P = 2^+$ fraction above 0.67 at the 95% CL. The expected exclusion covers $J^P = 0^-$ ($J^P = 2^+$) fractions above 0.54 (0.47).

PACS numbers: 14.80.Bn, 14.80.Ec, 13.85.Rm

After the discovery of a Higgs boson, H , at the CERN Large Hadron Collider (LHC) [1, 2] in bosonic final states, and evidence for its decay to a pair of b quarks at the Tevatron experiments [3], and to pairs of fermions at the CMS experiment [4], it is important to determine the new particle's properties using all decay modes available. In particular, the spin and parity of the Higgs boson are important in determining the framework of the mass generation mechanism. The SM predicts that the Higgs boson is a CP-even spin-0 particle ($J^P = 0^+$). If the

Higgs boson is indeed a single boson, the observation of its decay to two photons at the LHC precludes spin 1 according to the Landau-Yang theorem [5, 6]. Other J^P possibilities are possible. An admixture of $J^P = 0^+$ and $J^P = 0^-$ can arise in Two-Higgs-Doublet models (2HDM) [7, 8] of type II such as found in supersymmetric models. A boson with tensor couplings ($J^P = 2^+$) can arise in models with extra dimensions [9]. The ATLAS and CMS Collaborations have examined the possibility that the H boson has $J^P = 0^-$ or $J^P = 2^+$ using its decays to $\gamma\gamma$, ZZ , and WW states [10–14]. The $J^P = 0^-$ hypothesis is excluded at the 97.8% and 99.95% CL by the ATLAS and CMS Collaborations, respectively, in the $H \rightarrow ZZ \rightarrow 4\ell$ decay mode. Likewise, the $J^P = 2^+$ hypothesis is excluded at the $\geq 99.9\%$ CL by the ATLAS Collaboration when combining all bosonic decay modes, and at the $\geq 97.7\%$ CL by the CMS Collaboration in the $H \rightarrow ZZ \rightarrow 4\ell$ decay mode (depending on the production processes and the quark-mediated fraction of the production processes). However, the J^P character of Higgs bosons decaying to pairs of fermions, and in particular to $b\bar{b}$, has not yet been studied. In this Letter we present tests of non-SM models describing produc-

*with visitors from ^aAugustana College, Sioux Falls, SD, USA, ^bThe University of Liverpool, Liverpool, UK, ^cDESY, Hamburg, Germany, ^dUniversidad Michoacana de San Nicolas de Hidalgo, Morelia, Mexico ^eSLAC, Menlo Park, CA, USA, ^fUniversity College London, London, UK, ^gCentro de Investigacion en Computacion - IPN, Mexico City, Mexico, ^hUniversidade Estadual Paulista, São Paulo, Brazil, ⁱKarlsruher Institut für Technologie (KIT) - Steinbuch Centre for Computing (SCC), D-76128 Karlsruhe, Germany, ^jOffice of Science, U.S. Department of Energy, Washington, D.C. 20585, USA, ^kAmerican Association for the Advancement of Science, Washington, D.C. 20005, USA, ^lKiev Institute for Nuclear Research, Kiev, Ukraine and ^mUniversity of Maryland, College Park, Maryland 20742, USA.

tion of bosons with a mass of 125 GeV, $J^P = 0^-$ or $J^P = 2^+$, and decaying to $b\bar{b}$. We explore two scenarios for each of the hypotheses: (a) the new boson is a $J^P = 0^-$ ($J^P = 2^+$) particle and (b) the observed resonance is either a combination of these non-SM J^P states and a $J^P = 0^+$ state or distinct states with degenerate mass. In the latter case, we do not consider interference effects between states.

Unlike the LHC J^P measurements, our ability to distinguish different Higgs boson J^P assignments is not based primarily on the angular analysis of the Higgs boson decay products. It is instead based on the kinematic correlations between the vector boson V ($V = W, Z$) and the Higgs boson in VH associated production. Searches for associated VH production are sensitive to the different kinematics of the various J^P combinations in several observables, especially the invariant mass of the VH system, due to the dominant p and d wave contributions to the $J^P = 0^-$ and $J^P = 2^+$ production processes [15–17]. The p and d wave contributions to the production cross sections near threshold vary as β^3 and β^5 , respectively, whereas the s wave contribution for the SM Higgs boson varies as β , where β is the ratio of the Higgs boson momentum and energy.

To test compatibility of non-SM J^P models with data we use the D0 studies of $ZH \rightarrow \ell\ell b\bar{b}$ [18], $WH \rightarrow \ell\nu b\bar{b}$ [19], and $ZH \rightarrow \nu\nu b\bar{b}$ [20] with no modifications to the event selections. Lepton flavors considered in the $WH \rightarrow \ell\nu b\bar{b}$ and $ZH \rightarrow \ell\ell b\bar{b}$ analyses include electrons and muons. Events with taus that decay to these leptons are considered as well, although their contribution is small. The D0 detector is described in Refs. [21–23].

We use 9.5–9.7 fb $^{-1}$ of integrated luminosity collected with the D0 detector satisfying relevant data-quality requirements in each of the three analyses. The SM background processes are either estimated from dedicated data samples (multijet backgrounds), or from Monte Carlo (MC) simulation. The V +jets and $t\bar{t}$ processes are generated using ALPGEN [24], single top processes are generated using SINGLETOP [25], and diboson (VV) processes are generated using PYTHIA [26]. The SM Higgs boson processes are also generated using PYTHIA. The signal samples for the $J^P = 0^-$ and $J^P = 2^+$ hypotheses are generated using MADGRAPH 5 [27]. We have verified that $J^P = 0^+$ samples produced with MADGRAPH agree well with the SM PYTHIA prediction.

In the following, we denote a non-SM Higgs boson as X , reserving the label H for the SM $J^P = 0^+$ Higgs boson. MADGRAPH can simulate several non-SM models, as well as user-defined models. These new states are introduced via dimension-5 Lagrangian operators [16]. The $J^P = 0^-$ samples are created using a model from the authors of Ref. [15]. The non-SM Lagrangian can be expressed as [16] $\mathcal{L}_{0^-} = \frac{c_V^A}{\Lambda} A F_{\mu\nu} \tilde{F}^{\mu\nu}$, where $F_{\mu\nu}$ is the field-strength tensor for the vector boson, A is the new

boson field, c_V^A is a coupling term, and Λ is the scale at which new physics effects arise. The $J^P = 2^+$ signal samples are created using a Randall-Sundrum (RS) model, an extra-dimension model with a massive $J^P = 2^+$ particle that has graviton-like couplings [28–31]. This model’s Lagrangian can be expressed as $\mathcal{L}_{2^+} = \frac{c_V^G}{\Lambda} G^{\mu\nu} T_{\mu\nu}$, where $G^{\mu\nu}$ represents the $J^P = 2^+$ particle, c_V^G is a coupling term, $T_{\mu\nu}$ is the stress-energy tensor of the vector boson, and Λ is the effective Planck mass [9]. The mass of the non-SM Higgs-like particle X is set to 125 GeV, a value close to the mass measured by the LHC Collaborations [1, 2] and also consistent with measurements at the Tevatron [3]. We study the decay of X to $b\bar{b}$ only. For our initial sample normalization we assume that the ratio μ of the product of the cross section and the branching fraction, $\sigma(VX) \times \mathcal{B}(X \rightarrow b\bar{b})$, to the SM prediction is $\mu = 1.0$ [32, 33], and subsequently define exclusion regions as functions of μ . We use the CTEQ6L1 PDF set for sample generation, and PYTHIA for parton showering and hadronization. The MC samples are processed by the full D0 detector simulation. To reproduce the effect of multiple $p\bar{p}$ interactions in the same beam crossing, each simulated event is overlaid with an event from a sample of random beam crossings with the same instantaneous luminosity profile as the data. The events are then reconstructed with the same programs as the data.

All three analyses employ a b -tagging algorithm based on track impact parameters, secondary vertices, and event topology to select jets that are consistent with originating from a b quark [34, 35].

The $ZH \rightarrow \ell\ell b\bar{b}$ analysis [18] selects events with two isolated charged leptons and at least two jets. A kinematic fit corrects the measured jet energies to their best fit values based on the constraints that the dilepton invariant mass should be consistent with the Z boson mass [36] and that the total transverse momentum of the leptons and jets should be consistent with zero. The event sample is further divided into orthogonal “single-tag” (ST) and “double-tag” (DT) channels according to the number of b -tagged jets. The SM Higgs boson search uses random forest (RF) [37] discriminants to provide distributions for the final statistical analysis. The first RF is designed to discriminate against $t\bar{t}$ events and divides events into $t\bar{t}$ -enriched and $t\bar{t}$ -depleted ST and DT regions. In this study only events in the $t\bar{t}$ -depleted ST and DT regions are considered. These regions contain $\approx 94\%$ of the SM Higgs signal.

The $WH \rightarrow \ell\nu b\bar{b}$ analysis [19] selects events with one charged lepton, significant imbalance in the transverse energy (\cancel{E}_T), and two or three jets. This search is also sensitive to the $ZH \rightarrow \ell\ell b\bar{b}$ process when one of the charged leptons is not identified. Using the outputs of the b -tagging algorithm for all selected jets, events are divided into four orthogonal b -tagging categories, “one-tight-tag” (1TT), “two-loose-tag” (2LT), “two-medium-

tag” (2MT), and “two-tight-tag” (2TT). Looser b -tagging categories correspond to higher efficiencies for true b quarks and higher fake rates. Outputs from boosted decision trees (BDTs) [37], trained separately for each jet multiplicity and tagging category, serve as the final discriminants in the SM Higgs boson search.

The $ZH \rightarrow \nu\nu b\bar{b}$ analysis [20] selects events with large \cancel{E}_T and exactly two jets. This search is also sensitive to the WH process when the charged lepton from the $W \rightarrow \ell\nu$ decay is not identified. A dedicated BDT is used to provide rejection of the large multijet background. Two orthogonal b -tagging channels, medium (MT), and tight (TT), use the sum of the b -tagging discriminants of the two selected jets. BDT classifiers, trained separately for the different b -tagging categories, provide the final discriminants in the SM Higgs boson search.

These three analyses are among the inputs to the D0 SM Higgs boson search [38], yielding an excess above the SM background expectation that is consistent both in shape and in magnitude with a SM Higgs boson signal. The best fit to data for the $H \rightarrow b\bar{b}$ decay channel for the product of the signal cross section and branching fraction, is $\mu = 1.23^{+1.24}_{-1.17}$ for a mass of 125 GeV. When including data from both Tevatron experiments, the best fit to data yields $\mu = 1.59^{+0.69}_{-0.72}$ [39].

Discrimination between the J^P values of non-SM and SM hypotheses is achieved by using mass information of the VX system. For the $\ell\ell b\bar{b}$ final state we use the invariant mass of the two leptons and either the two highest b -tagged jets (DT) or the b -tagged jet and the highest p_T non-tagged jet (ST) as the final discriminating variable. For the final states that have neutrinos, the discriminating variable is the transverse mass of the VX system which is defined as $M_T^2 = (E_T^V + E_T^X)^2 - (\vec{p}_T^V + \vec{p}_T^X)^2$ where the transverse momenta of the Z and W bosons are $\vec{p}_T^Z = \vec{\cancel{E}}_T$ and $\vec{p}_T^W = \vec{\cancel{E}}_T + \vec{p}_T^\ell$. For the $\ell\nu b\bar{b}$ final state the two jets can either be one b -tagged jet (1TT) and the highest p_T non-tagged jet, or the two b -tagged jets from any of the other three b -tagging categories: 2LT, 2MT, or 2TT.

To improve the discrimination between the non-SM signals and backgrounds in the $\ell\ell b\bar{b}$ and $\nu\nu b\bar{b}$ final states, we use the invariant mass of the dijet system, M_{jj} , to select two regions with different signal purities. Events with dijet masses in the range $100 \leq M_{jj} \leq 150$ GeV ($70 \leq M_{jj} < 150$ GeV) for $\ell\ell b\bar{b}$ ($\nu\nu b\bar{b}$) final states comprise the “high-purity” region (HP), while the remaining events are in the “low-purity region” (LP). As a result of the kinematic fit, the HP region for the $\ell\ell b\bar{b}$ final state is narrower than that for the $\nu\nu b\bar{b}$ final state, given the correspondingly narrower dijet mass peak. For the $\ell\nu b\bar{b}$ final state we use the final BDT output (\mathcal{D}) of the SM Higgs boson search [19]. Since events with $\mathcal{D} \leq 0$ provide negligible sensitivity to SM or non-SM signals, we do not consider them further. We separate the remaining events into two categories with different signal purities. The LP

category consists of events with $0 \leq \mathcal{D} \leq 0.5$, and the HP category of events with $\mathcal{D} > 0.5$.

Figure 1 illustrates the discriminating variables for the three analysis channels in the high-purity categories for the most sensitive b -tagging selections. Distributions for additional subchannels can be found in Ref. [40].

We perform the statistical analysis using a modified frequentist approach [38, 41, 42]. We use a negative log-likelihood ratio (LLR) as the test statistic for two hypotheses: the null hypothesis, H_0 , and the test hypothesis, H_1 . This LLR is given by $\text{LLR} = -2 \ln(L_{H_1}/L_{H_0})$, where L_{H_x} is the joint likelihood for hypothesis x evaluated over the number of bins in the final discriminating variable distribution in each channel. To decrease the effect of systematic uncertainties on the sensitivity, we fit the signals and backgrounds by maximizing the likelihood functions by allowing the systematic effects to vary within Gaussian constraints. This fit is performed separately for both the H_0 and H_1 hypotheses for the data and each pseudo-experiment.

We define CL_s as CL_{H_1}/CL_{H_0} where CL_{H_x} for a given hypothesis H_x is $CL_{H_x} = P_{H_x}(\text{LLR} \geq \text{LLR}^{\text{obs}})$, and LLR^{obs} is the LLR value observed in the data. P_{H_x} is defined as the probability that the LLR falls beyond LLR^{obs} for the distribution of LLR populated by the H_x model. For example, if $CL_s \leq 0.05$ we exclude the H_1 hypothesis in favor of the H_0 hypothesis at $\geq 95\%$ CL.

Systematic uncertainties affecting both shape and rate are considered. The systematic uncertainties for each individual analysis are described in Refs. [18–20]. A summary of the major contributions follows. The largest contribution for all analyses is from the uncertainties on the cross sections of the simulated V + heavy-flavor jets backgrounds which are 20%–30%. All other cross section uncertainties for simulated backgrounds are less than 10%. Since the multijet background is estimated from data, its uncertainty depends on the size of the data sample from which it is estimated, and ranges from 10% to 30%. All simulated samples for the $WH \rightarrow \ell\nu b\bar{b}$ and $ZH \rightarrow \nu\nu b\bar{b}$ analyses have an uncertainty of 6.1% from the integrated luminosity [43], whereas the simulated samples from the $ZH \rightarrow \ell\ell b\bar{b}$ analysis have uncertainties ranging from 0.7%–7% arising from the fitted normalization to the data [18]. All analyses take into account uncertainties on the jet energy scale, resolution, and jet identification efficiency for a combined uncertainty of $\approx 7\%$. The uncertainty on the b -tagging rate varies from 1%–10% depending on the number and quality of the tagged jets. The correlations between the three analyses are described in Ref. [38].

In this Letter, the H_0 hypothesis always contains SM background processes and the SM Higgs boson normalized to $\mu \times \sigma_{0+}^{SM}$. To test the non-SM cross section we assign the H_1 hypothesis as the sum of the $J^P = 0^-$ or $J^P = 2^+$ signal plus SM background processes, with no contribution from the SM Higgs boson. We calculate

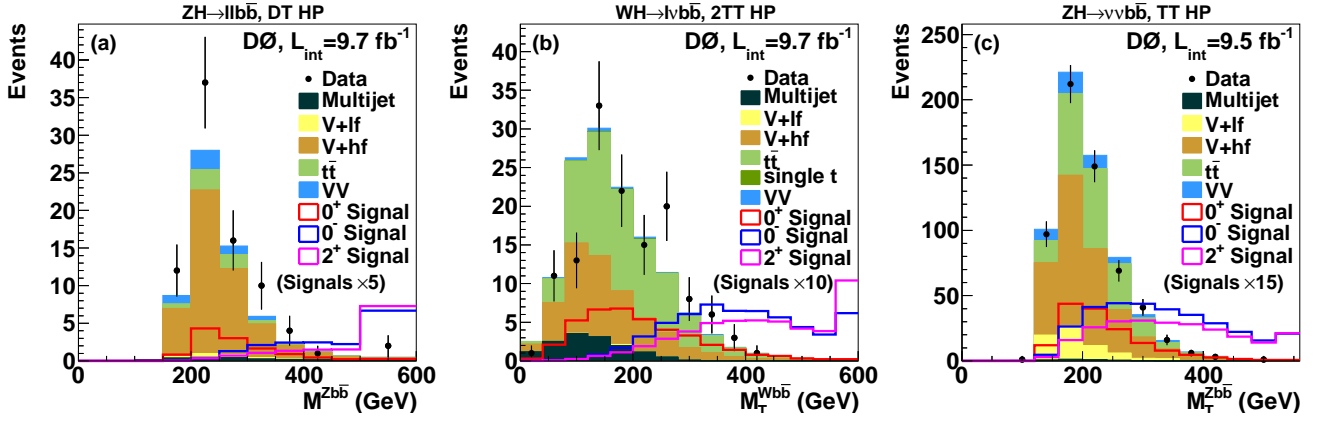


FIG. 1: (color online) (a) Invariant mass of the $\ell\ell b\bar{b}$ system in the $ZH \rightarrow \ell\ell b\bar{b}$ high-purity double-tag (DT HP) channel, (b) transverse mass of the $\ell\nu b\bar{b}$ system in the $WH \rightarrow \ell\nu b\bar{b}$ high-purity 2-tight-tag (2TT HP) channel, and (c) transverse mass of the $\nu\nu b\bar{b}$ system in the $ZH \rightarrow \nu\nu b\bar{b}$ high-purity tight-tag (TT HP) channel. The $J^P = 0^-$ and $J^P = 2^+$ samples are normalized to the product of the SM cross section and branching fraction multiplied by an additional factor. Heavy- and light-flavor quark jets are denoted by lf and hf, respectively. Overflow events are included in the highest mass bin. For all signals, a mass of 125 GeV for the H or X boson is assumed.

the CL_s values using signal cross sections expressed as $\mu \times \sigma_{0^+}^{SM}$ and evaluate the expected values for each of these quantities by replacing LLR^{obs} with $LLR_{0^+}^{exp}$, the median expectation for the $J^P = 0^+$ hypothesis only. Figure 2 illustrates the LLR distributions for the H_0 and $J^P = 2^+$ H_1 hypotheses, and the observed LLR value assuming $\mu = 1.0$, a production rate compatible with both Tevatron and LHC Higgs boson measurements. The similar plot for $J^P = 0^-$ is shown in Ref. [40]. We interpret $1 - CL_s$ as the confidence level at which we exclude the non-SM hypothesis for the models considered in favor of the SM prediction of $J^P = 0^+$ for the given value of μ . For $\mu = 1.0$ we exclude the $J^P = 0^-$ ($J^P = 2^+$) hypothesis at the 97.6% (99.0%) CL. The expected exclusions are at the 99.86% and 99.94% CL. Results, including those for $\mu = 1.23$, are given in Table I.

Tables detailing the CL_{H_x} values for each individual analysis channel and the combination can be found in Ref. [40]. We also obtain $1 - CL_s$ over a range of SM and non-SM signal strengths. Figure 3 shows the expected and observed 95% CL exclusions as a function of the $J^P = 0^-$ ($J^P = 2^+$) and $J^P = 0^+$ signal strengths, which may differ between the SM and non-SM signals. In the tests shown in Fig. 3 the signal in the H_1 hypothesis is the $J^P = 0^-$ ($J^P = 2^+$) signal normalized to μ_{0^-} (μ_{2^+}) $\times \sigma_{0^+}^{SM}$, and the signal in the H_0 hypothesis is the $J^P = 0^+$ signal normalized to $\mu_{0^+} \times \sigma_{0^+}^{SM}$.

We also consider the possibility of a combination of J^P signals in our data (e.g., $J^P = 0^+$ and $J^P = 0^-$). These tests provide constraints on a number of theoretical models such as those containing pseudoscalar bosons in addition to a SM-like Higgs boson. For these studies we fix the sum of the two cross sections to a specific value of $\mu \times \sigma_{0^+}^{SM}$ and vary the fractions $f_{0^-} = \sigma_{0^-}/(\sigma_{0^+} + \sigma_{0^-})$ or $f_{2^+} = \sigma_{2^+}/(\sigma_{0^+} + \sigma_{2^+})$ of non-SM signal and calcu-

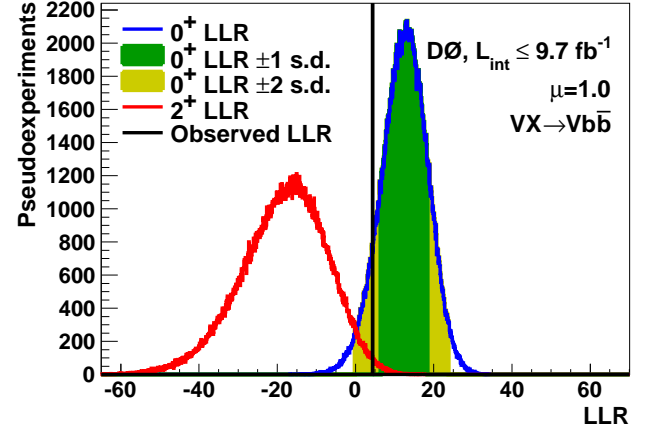


FIG. 2: (color online) LLR distributions comparing the $J^P = 0^+$ and the $J^P = 2^+$ hypotheses for the combination. The $J^P = 0^+$ and $J^P = 2^+$ samples are normalized to the product of the SM cross section and branching fraction. The vertical solid line represents the observed LLR value assuming $\mu = 1.0$, while the dark and light shaded areas represent the 1 and 2 standard deviations (s.d.) on the expectation from the null hypothesis H_0 , respectively.

late the same CL_s values as above as a function of f_{0^-} or f_{2^+} . To study f_{0^-} , we now modify H_1 to be the sum of the background, the $J^P = 0^-$ signal normalized to $\mu \times \sigma_{0^+}^{SM} \times f_{0^-}$, and the $J^P = 0^+$ signal normalized to $\mu \times \sigma_{0^+}^{SM} \times (1 - f_{0^-})$. H_0 remains as previously defined. We follow an identical prescription for $J^P = 2^+$. Figure 4 presents the value $1 - CL_s$ as a function of the $J^P = 0^-$ signal fraction f_{0^-} for the case of $\mu = 1.0$, and the corresponding figure for the $J^P = 2^+$ hypothesis is available in Ref. [40]. For $\mu = 1.0$ we exclude a $J^P = 0^-$ ($J^P = 2^+$) signal fraction $f_{0^-} > 0.80$ ($f_{2^+} > 0.67$) at the 95% CL.

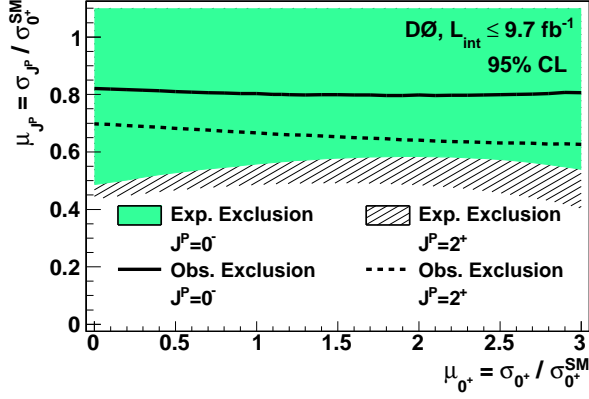


FIG. 3: (color online) The expected exclusion region (shaded area) and observed exclusion (solid line) as functions of the $J^P = 0^-$ and $J^P = 0^+$ signal strengths. The expected exclusion region (hatched area) and observed exclusion (dashed line) as functions of the $J^P = 2^+$ and $J^P = 0^+$ signal strengths.

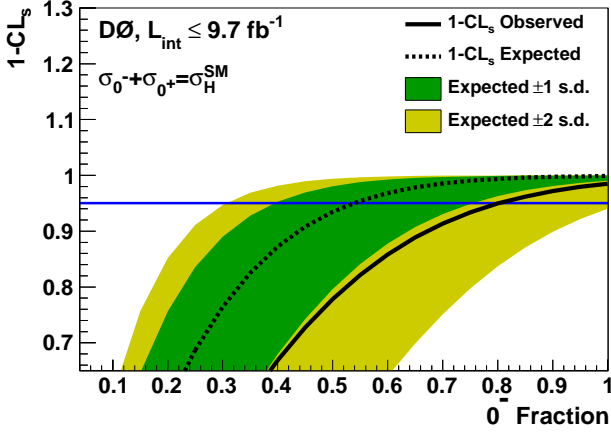


FIG. 4: (color online) $1 - CL_s$ as a function of the $J^P = 0^-$ signal fraction assuming the product of the total cross section and branching ratio is equal to the SM prediction. The horizontal blue line corresponds to the 95% CL exclusion. The dark and light shaded regions represent the 1 and 2 standard deviations (s.d.) fluctuations for the $J^P = 0^+$ hypothesis.

The expected exclusions are $f_{0^-} > 0.54$ ($f_{2^+} > 0.47$). Limits on admixture fractions for other choices of μ are shown in [40].

In summary, we have performed tests of models with non-SM spin and parity assignments in Higgs boson production with a W or Z boson and decaying into $b\bar{b}$ pairs. We use the published analyses of the $WH \rightarrow \ell\nu b\bar{b}$, $ZH \rightarrow \ell\ell b\bar{b}$, and $ZH \rightarrow \nu\nu b\bar{b}$ final states with no modifications to the event selections. Sensitivity to non-SM J^P assignments in the two models considered here is enhanced via the separation of samples into high- and low-purity categories wherein the total mass or total transverse mass of the VX system provides powerful discrim-

ination. Assuming a production rate compatible with both Tevatron and LHC Higgs boson measurements, our data strongly reject non-SM J^P predictions, and agree with the SM $J^P = 0^+$ prediction. Under the assumption of two nearly degenerate bosons with different J^P values, we set upper limits on the fraction of non-SM signal in our data. This is the first exclusion of non-SM J^P parameter space in a fermionic decay channel of the Higgs boson.

J^P	$1 - CL_s$ (s.d.)		f_{J^P}	
$\mu = 1.0$	Exp.	Obs.	Exp.	Obs.
0^-	0.9986 (3.00)	0.976 (1.98)	>0.54	>0.80
2^+	0.9994 (3.22)	0.990 (2.34)	>0.47	>0.67
$\mu = 1.23$				
0^-	0.9998 (3.60)	0.995 (2.56)	>0.45	>0.67
2^+	0.9999 (3.86)	0.998 (2.91)	>0.40	>0.56

TABLE I: Expected and observed $1 - CL_s$ values (converted to s.d. in parentheses) and signal fractions for $\mu = 1.0$ and $\mu = 1.23$ excluded at the 95% CL.

We thank the staffs at Fermilab and collaborating institutions, and acknowledge support from the DOE and NSF (USA); CEA and CNRS/IN2P3 (France); MON, NRC KI and RFBR (Russia); CNPq, FAPERJ, FAPESP and FUNDUNESP (Brazil); DAE and DST (India); Colciencias (Colombia); CONACyT (Mexico); NRF (Korea); FOM (The Netherlands); STFC and the Royal Society (United Kingdom); MSMT and GACR (Czech Republic); BMBF and DFG (Germany); SFI (Ireland); The Swedish Research Council (Sweden); and CAS and CNSF (China).

- [1] G. Aad *et al.* [ATLAS Collaboration], Phys. Lett. B **716**, 1 (2012).
- [2] S. Chatrchyan *et al.* [CMS Collaboration], Phys. Lett. B **716**, 30 (2012).
- [3] T. Aaltonen *et al.* [CDF and D0 Collaborations], Phys. Rev. Lett. **109**, 071804 (2012).
- [4] S. Chatrchyan *et al.*, [CMS Collaboration], Nat. Phys. **10**, 557 (2014).
- [5] L. Landau, Dokl. Akad. Nauk Ser. Fiz. **60**, 207 (1948).
- [6] C. N. Yang, Phys. Rev. **77**, 242 (1950).
- [7] T. D. Lee, Phys. Rev. D **8**, 1226 (1973).
- [8] E. Cerveró and J.-M. Gérard, Phys. Lett. B **712**, 255 (2012).
- [9] R. Fok, C. Guimaraes, R. Lewis, and V. Sanz, J. High Energy Phys. **12**, 062 (2012).
- [10] S. Chatrchyan *et al.* [CMS Collaboration], Phys. Rev. Lett. **110**, 081803 (2013).
- [11] G. Aad *et al.* [ATLAS Collaboration], Phys. Lett. B **726**, 120 (2013).

- [12] S. Chatrchyan *et al.* [CMS Collaboration], J. High Energy Phys. **01**, 096 (2014).
- [13] S. Chatrchyan *et al.* [CMS Collaboration], Phys. Rev. D **89**, 092007 (2014).
- [14] S. Chatrchyan *et al.* [CMS Collaboration], arXiv:1407.0558, (2014), submitted to Eur. Phys. J. C.
- [15] J. Ellis, D. S. Hwang, V. Sanz, and T. You, J. High Energy Phys. **12**, 134 (2012).
- [16] J. Ellis, V. Sanz, and T. You, Eur. Phys. J. C **73** (2013).
- [17] D. Miller, S. Choi, B. Eberle, M. Mühlleitner, and P. Zerwas, Phys. Lett. B **505**, 149 (2001).
- [18] V. M. Abazov *et al.* [D0 Collaboration], Phys. Rev. D **88**, 052010 (2013).
- [19] V. M. Abazov *et al.* [D0 Collaboration], Phys. Rev. D **88**, 052008 (2013).
- [20] V. M. Abazov *et al.* [D0 Collaboration], Phys. Lett. B **716**, 285 (2012).
- [21] V. M. Abazov *et al.* [D0 Collaboration], Nucl. Instrum. Methods Phys. Res. A **565**, 463 (2006).
- [22] M. Abolins *et al.*, Nucl. Instrum. Methods Phys. Res. A **584**, 75 (2008).
- [23] R. Angstadt *et al.*, Nucl. Instrum. Methods Phys. Res. A **622**, 298 (2010).
- [24] M. L. Mangano, M. Moretti, F. Piccinini, R. Pittau, and A. D. Polosa, J. High Energy Phys. **07**, 001 (2003).
- [25] E. E. Boos, V. E. Bunichev, L. V. Dudko, V. I. Savrin, and V. V. Sherstnev, Phys. Atom. Nucl. **69**, 1317 (2006).
- [26] T. Sjöstrand, S. Mrenna, and P. Z. Skands, J. High Energy Phys. **05**, 026 (2006).
- [27] J. Alwall, M. Herquet, F. Maltoni, O. Mattelaer, and T. Stelzer, J. High Energy Phys. **06**, 128 (2011). We use version 1.4.8.4.
- [28] L. Randall and R. Sundrum, Phys. Rev. Lett. **83**, 3370 (1999).
- [29] L. Randall and R. Sundrum, Phys. Rev. Lett. **83**, 4690 (1999).
- [30] K. Hagiwara, J. Kanzaki, Q. Li, and K. Mawatari, Eur. Phys. J. C **56**, 435 (2008).
- [31] P. Aquino, K. Hagiwara, Q. Li, and F. Maltoni, J. High Energy Phys. **11**, 1 (2011).
- [32] J. Baglio and A. Djouadi, J. High Energy Phys. **10**, 064 (2010).
- [33] O. Brein, R. V. Harlander, M. Wiesemann, and T. Zirke, Eur. Phys. J. C **72**, 1 (2012).
- [34] V. M. Abazov *et al.* [D0 Collaboration], Nucl. Instrum. Methods Phys. Res. A **763**, 290 (2014).
- [35] V. M. Abazov *et al.* [D0 Collaboration], Nucl. Instrum. Methods Phys. Res. A **620**, 490 (2010).
- [36] J. Beringer *et al.*, Particle Data Group, Phys. Rev. D **86**, 010001 (2012), and 2013 partial update for the 2014 edition.
- [37] A. Hoecker *et al.*, PoS **ACAT**, 040 (2007). We use version 4.1.0.
- [38] V. M. Abazov *et al.* [D0 Collaboration], Phys. Rev. D **88**, 052011 (2013).
- [39] T. Aaltonen *et al.* [CDF and D0 Collaborations], Phys. Rev. D **88**, 052014 (2013).
- [40] See Supplemental Material.
- [41] A. L. Read, J. Phys. G **28**, 2693 (2002).
- [42] W. Fisher, FERMILAB-TM-2386-E (2007).
- [43] T. Andeen *et al.*, FERMILAB-TM-2365 (2007).

SUPPLEMENTAL MATERIAL

In this document we provide supplemental information on the constraints on models with non-SM spin and parity for the Higgs boson in the $VH \rightarrow Vb\bar{b}$ final states in up to 9.7 fb^{-1} of $p\bar{p}$ collisions at $\sqrt{s} = 1.96 \text{ TeV}$ collected with the D0 detector at the Fermilab Tevatron Collider. We denote a non-SM Higgs boson as X .

Figure 5: Dijet mass distributions for the $\nu\nu b\bar{b}$ and $\ell\ell b\bar{b}$ analyses and the BDT output distribution for the $\ell\nu b\bar{b}$ analysis.

Figures 6–9: Additional VX invariant and transverse mass distributions for individual analyses.

Figures 10 and 11: LLR distributions for the individual analyses and their combination.

Tables II and III: Tables of CL_{H_x} and $1 - CL_s$ values for the individual analyses and their combination for $\mu = 1.0$ and $\mu = 1.23$.

Figure 12: $1 - CL_s$ as a function of the $J^P = 2^+$ signal fraction, f_{2^+} , for all analyses combined.

Figure 13: The expected and observed 95% CL exclusion as functions of the $J^P = 0^-$ ($J^P = 2^+$) signal fraction, f_{0^-} (f_{2^+}), and the total signal strength.

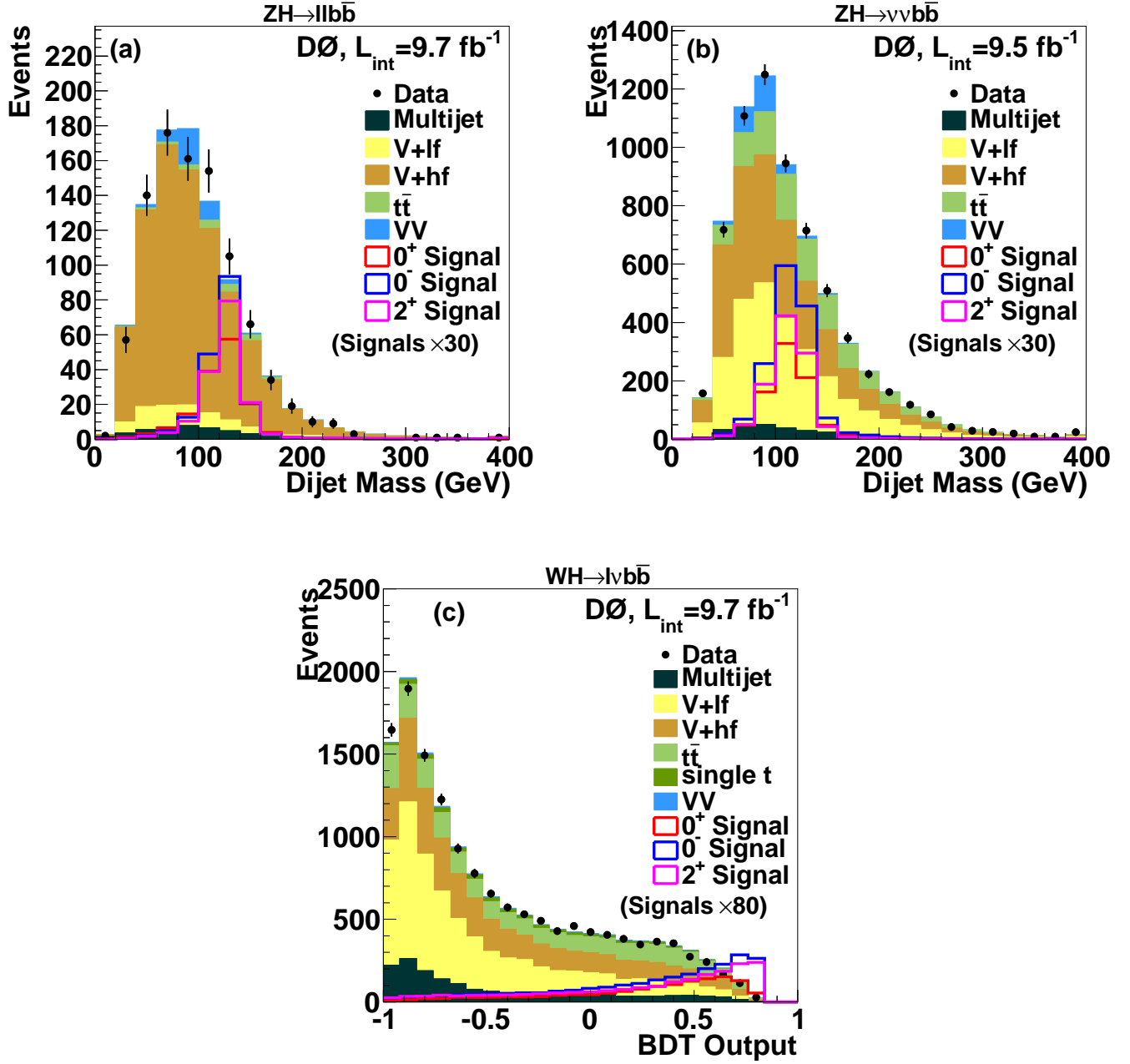


FIG. 5: Invariant mass of the dijet system for (a) the $ZH \rightarrow \ell\ell b\bar{b}$ analysis, and (b) the $ZH \rightarrow \nu\nu b\bar{b}$ analysis, and the BDT output for (c) the $WH \rightarrow \ell\nu b\bar{b}$ analysis. The $J^P = 2^+$ and $J^P = 0^-$ samples are normalized to the product of the SM cross section and branching fraction multiplied by an additional factor. Heavy- and light-flavor quark jets are denoted by lf and hf, respectively. Overflow events are included in the highest bin. For all signals, a mass of 125 GeV for the H or X boson is assumed.

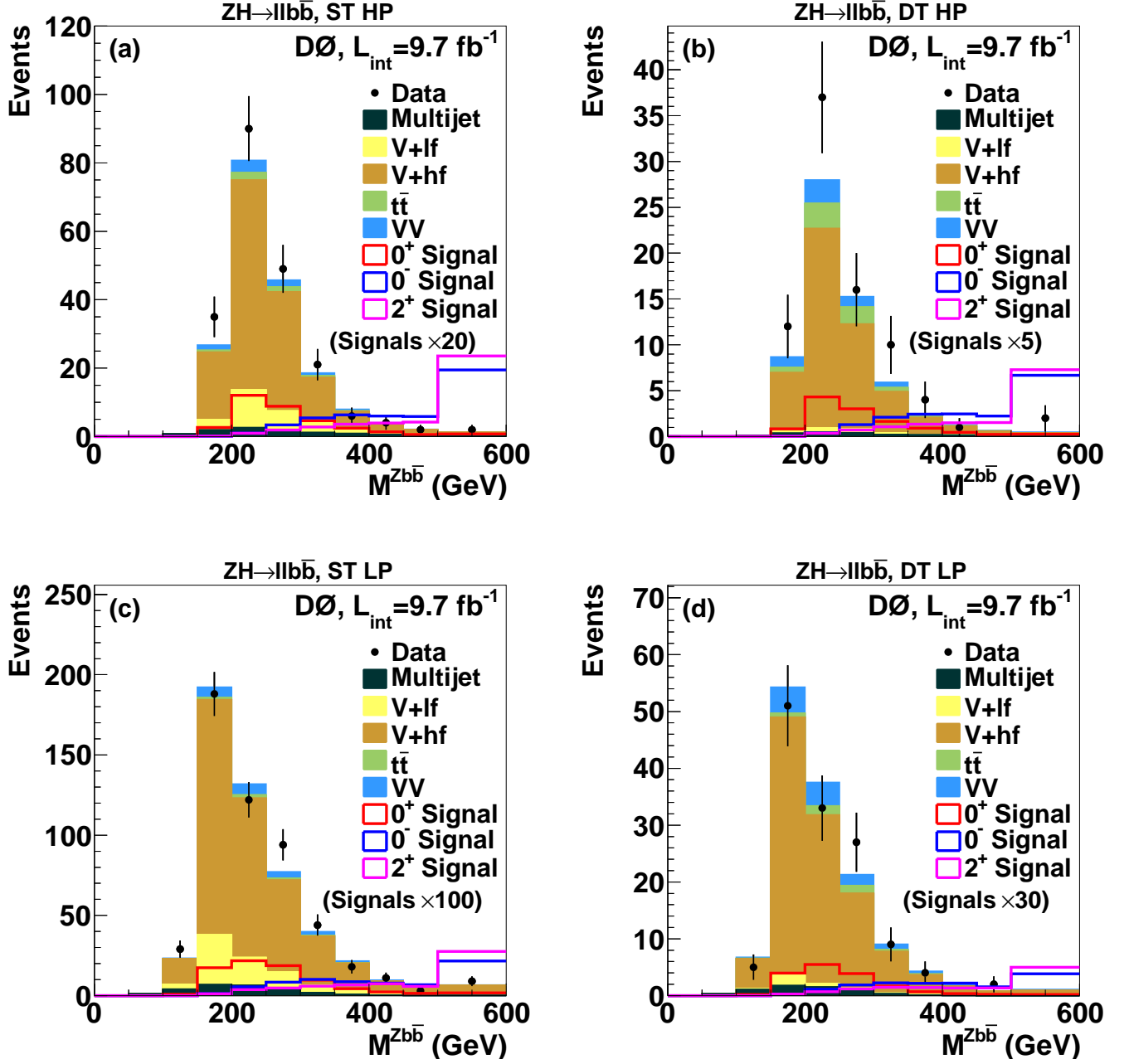


FIG. 6: Invariant mass of the $\ell\ell b\bar{b}$ system in the $ZH \rightarrow \ell\ell b\bar{b}$ analysis for events in the (a) single-tag high-purity (ST HP), (b) double-tag high-purity (DT HP), (c) single-tag low-purity (ST LP), and (d) double-tag low-purity (DT LP) channels. The $J^P = 2^+$ and $J^P = 0^-$ samples are normalized to the product of the SM cross section and branching fraction multiplied by an additional factor. Heavy- and light-flavor quark jets are denoted by lf and hf, respectively. Overflow events are included in the last bin. For all signals, a mass of 125 GeV for the H or X boson is assumed.

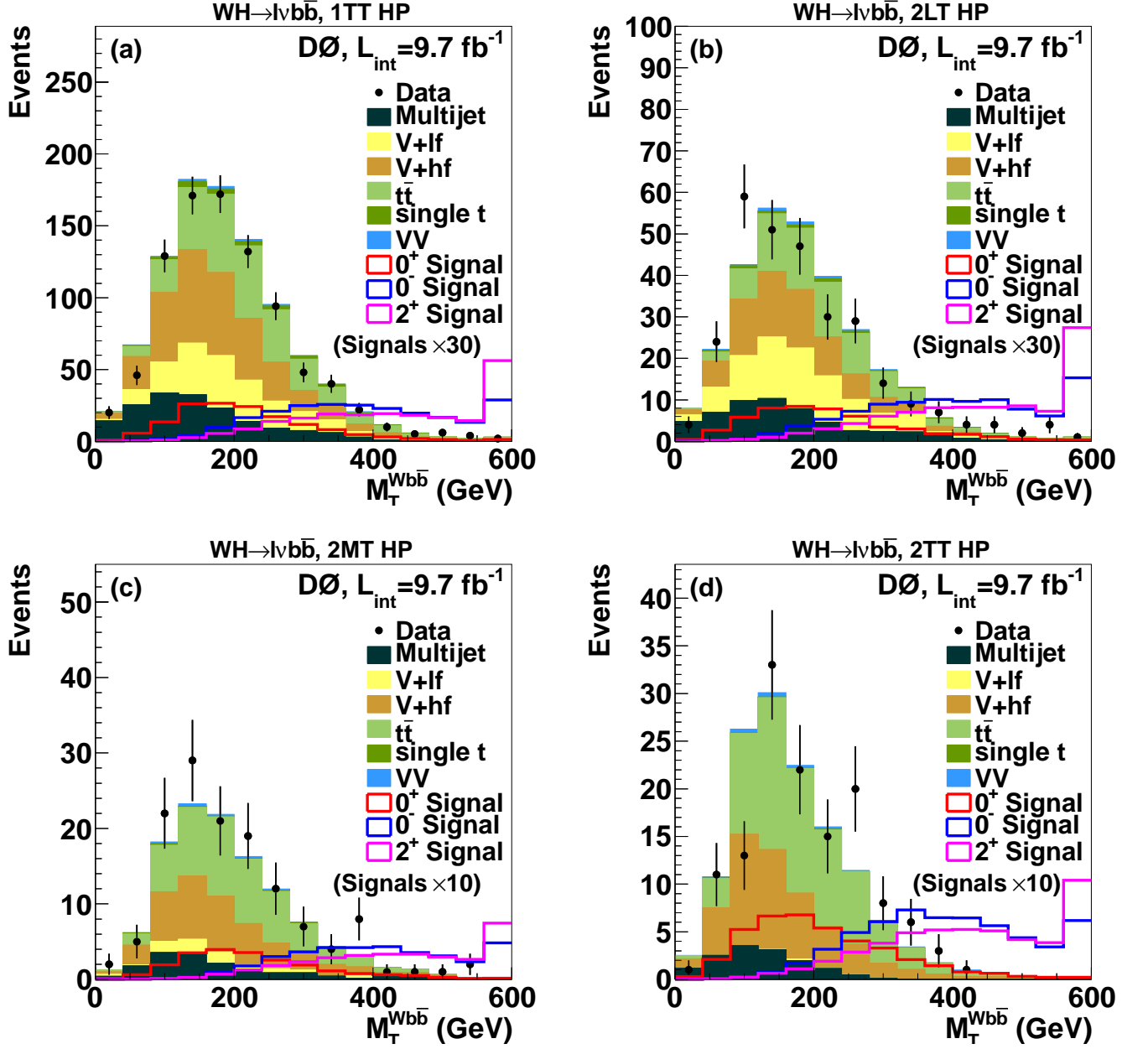


FIG. 7: Transverse mass of the $\ell\nu b\bar{b}$ system in the $WH \rightarrow \ell\nu b\bar{b}$ analysis in the high-purity (HP) region for (a) 1 tight-tag (1TT), (b) 2 loose-tags (2LT), (c) 2 medium-tags (2MT), and (d) 2 tight-tags (2TT) channels. The $J^P = 2^+$ and $J^P = 0^-$ samples are normalized to the product of the SM cross section and branching fraction multiplied by an additional factor. Heavy- and light-flavor quark jets are denoted by lf and hf, respectively. Overflow events are included in the last bin. For all signals, a mass of 125 GeV for the H or X boson is assumed.

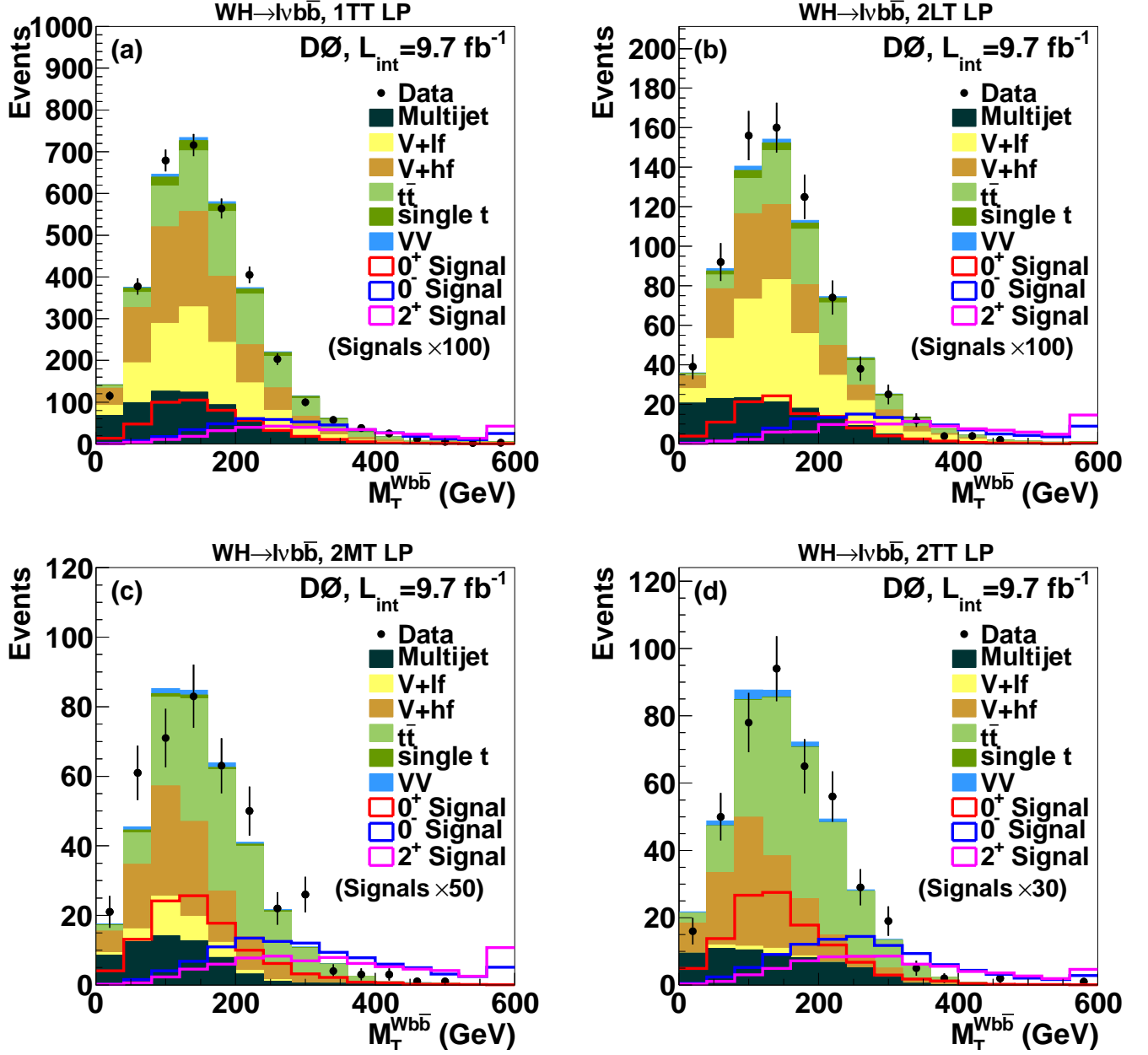


FIG. 8: Transverse mass of the $\ell\nu b\bar{b}$ system in the $WH \rightarrow \ell\nu b\bar{b}$ analysis in the low purity (LP) region for (a) 1-tight-tag (1TT), (b) 2-loose-tags (2LT), (c) 2-medium-tags (2MT), and (d) 2-tight-tags (2TT) channels. The $J^P = 2^+$ and $J^P = 0^-$ samples are normalized to the product of the SM cross section and branching fraction multiplied by an additional factor. Heavy- and light-flavor quark jets are denoted by lf and hf, respectively. Overflow events are included in the last bin. For all signals, a mass of 125 GeV for the H or X boson is assumed.

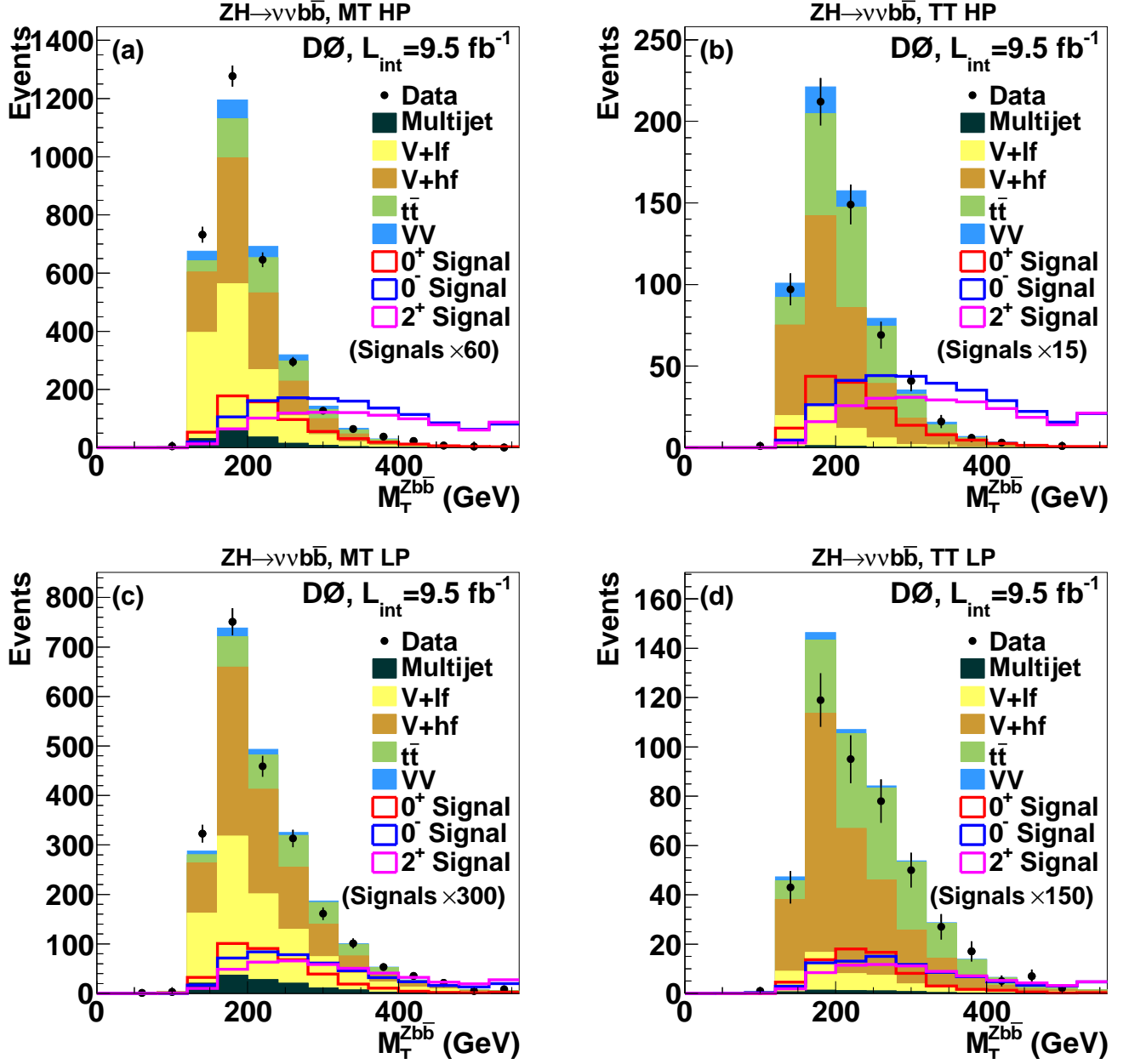


FIG. 9: Transverse mass of the $\nu\nu b\bar{b}$ system in the $ZH \rightarrow \nu\nu b\bar{b}$ analysis for events in the (a) medium-tag high-purity (MT HP), (b) tight-tag high-purity (TT HP), (c) medium-tag low-purity (MT LP), and (d) tight-tag low-purity (TT LP) channels. The $J^P = 2^+$ and $J^P = 0^-$ samples are normalized to the product of the SM cross section and branching fraction multiplied by an additional factor. Heavy- and light-flavor quark jets are denoted by lf and hf, respectively. Overflow events are included in the last bin. For all signals, a mass of 125 GeV for the H or X boson is assumed.

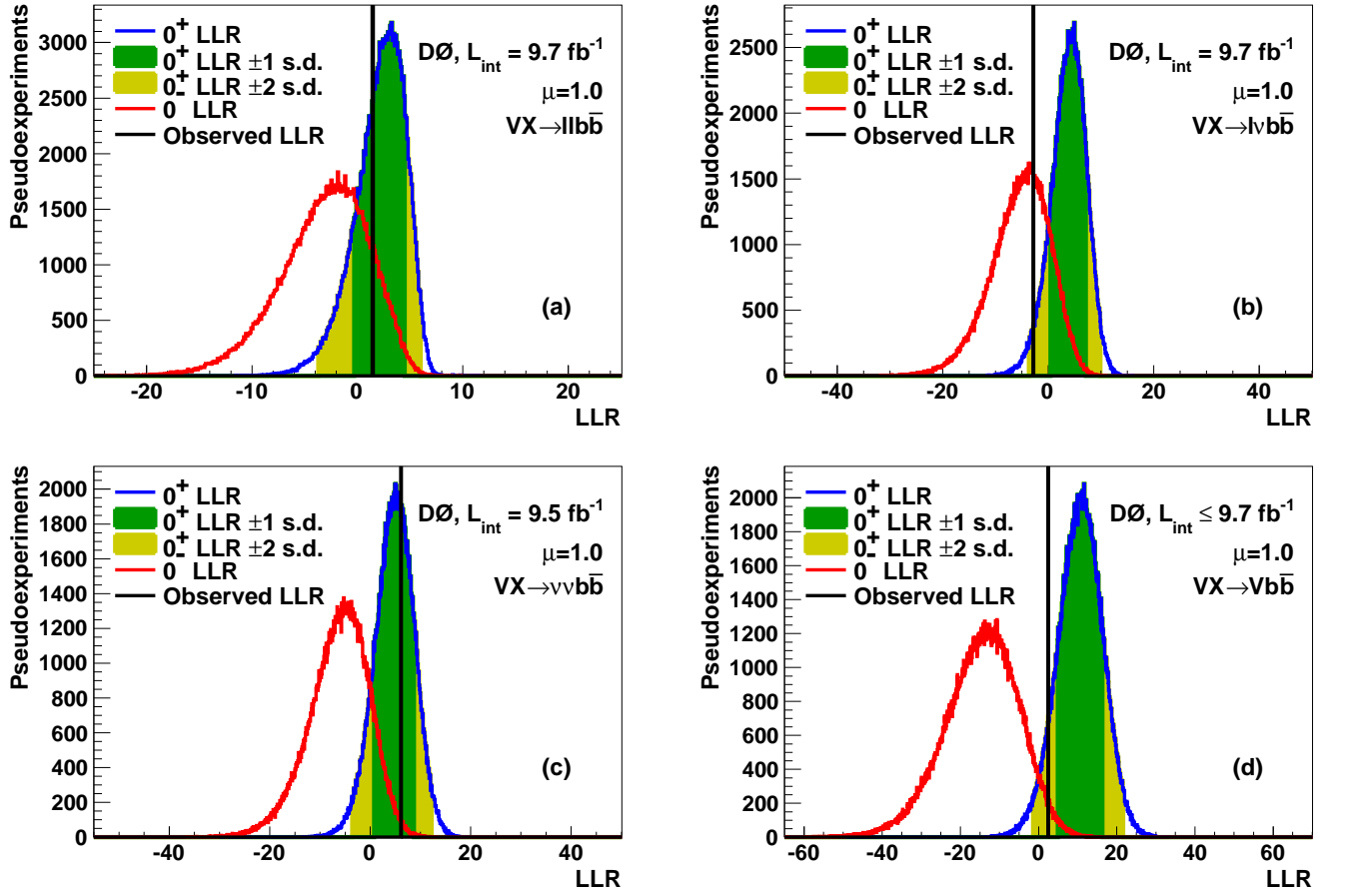


FIG. 10: LLR distributions comparing the $J^P = 0^+$ and the $J^P = 0^-$ hypotheses for the (a) $ZH \rightarrow \ell\ell b\bar{b}$ analysis, (b) $WH \rightarrow \ell\nu b\bar{b}$ analysis, (c) $ZH \rightarrow \nu\nu b\bar{b}$ analysis, and (d) their combination. The $J^P = 0^+$ and $J^P = 0^-$ samples are normalized to the product of the SM cross section and branching fraction multiplied by $\mu = 1.0$. The vertical solid line represents the observed LLR value, while the dark and light shaded areas represent 1 s.d. and 2 s.d. on the expectation from the null hypothesis H_0 , respectively. Here H_0 is the SM $J^P = 0^+$ signal plus backgrounds. For all signals, a mass of 125 GeV for the H or X boson is assumed.

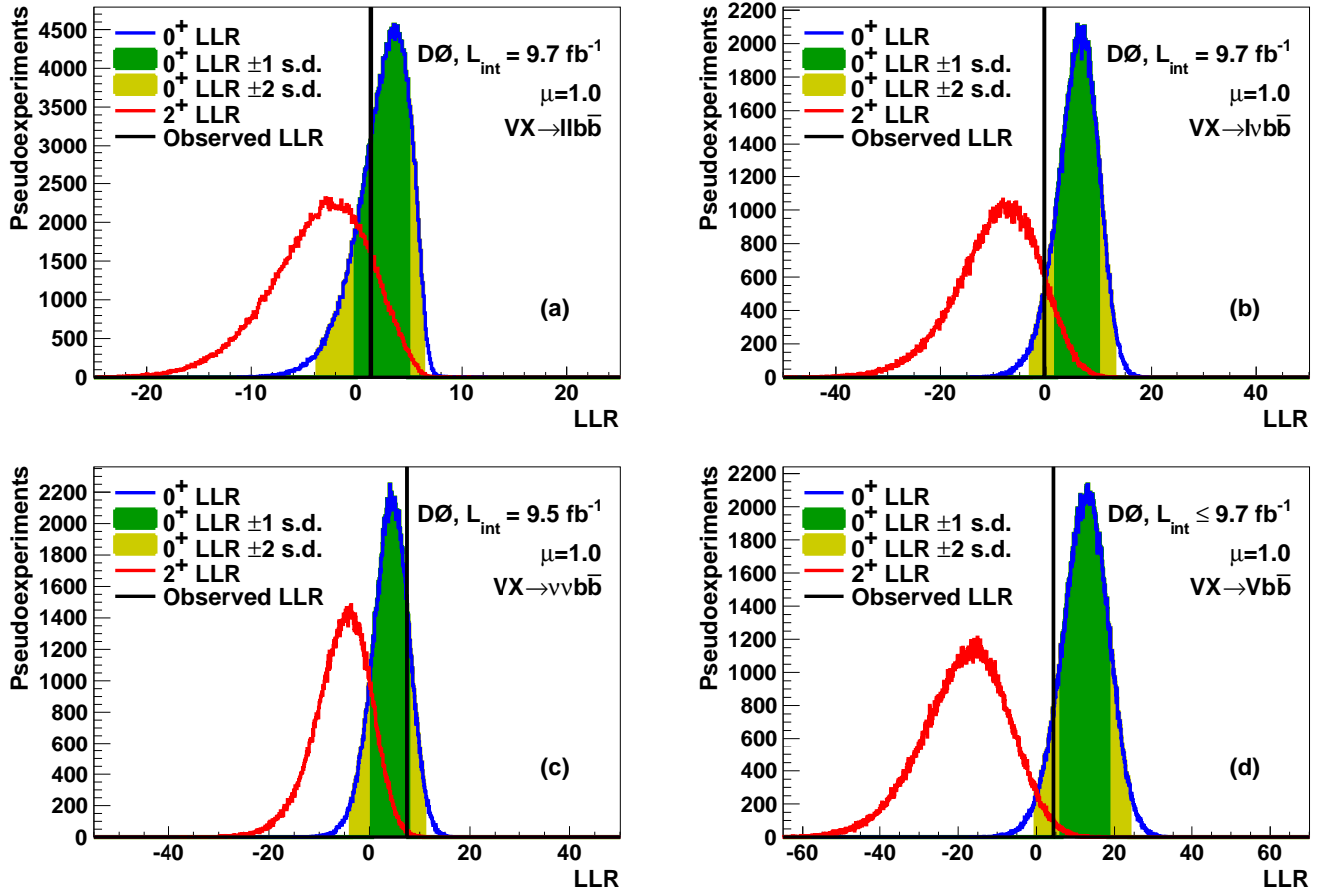


FIG. 11: LLR distributions comparing the $J^P = 0^+$ and the $J^P = 2^+$ hypotheses for the (a) $ZH \rightarrow \ell\ell b\bar{b}$ analysis, (b) $WH \rightarrow \ell\nu b\bar{b}$ analysis, (c) $ZH \rightarrow \nu\nu b\bar{b}$ analysis, and (d) their combination. The $J^P = 0^+$ and $J^P = 2^+$ samples are normalized to the product of the SM cross section and branching fraction multiplied by $\mu = 1.0$. The vertical solid line represents the observed LLR value, while the dark and light shaded areas represent 1 s.d. and 2 s.d. on the expectation from the null hypothesis H_0 , respectively. Here H_0 is the SM $J^P = 0^+$ signal plus backgrounds. For all signals, a mass of 125 GeV for the H or X boson is assumed.

Analysis	$ZH \rightarrow \ell\ell b\bar{b}$	$WH \rightarrow \ell\nu b\bar{b}$	$ZH \rightarrow \nu\nu b\bar{b}$	Combined
	$J^P = 0^-$ vs. $J^P = 0^+$			
CL_{0-} Expected	0.075	0.030	0.016	0.0007
CL_{0-} Observed	0.126	0.351	0.007	0.022
CL_{0+} Expected	0.500	0.500	0.500	0.500
CL_{0+} Observed	0.646	0.965	0.367	0.918
$1 - CL_s$ Expected	0.850 (1.04 s.d.)	0.941 (1.56 s.d.)	0.969 (1.87 s.d.)	0.9986 (3.00 s.d.)
$1 - CL_s$ Observed	0.805 (0.86 s.d.)	0.637 (0.35 s.d.)	0.981 (2.07 s.d.)	0.976 (1.98 s.d.)
	$J^P = 2^+$ vs. $J^P = 0^+$			
CL_{2+} Expected	0.064	0.009	0.023	0.0003
CL_{2+} Observed	0.134	0.114	0.002	0.009
CL_{0+} Expected	0.500	0.500	0.500	0.500
CL_{0+} Observed	0.702	0.932	0.173	0.906
$1 - CL_s$ Expected	0.872 (1.14 s.d.)	0.982 (2.09 s.d.)	0.953 (1.68 s.d.)	0.9994 (3.22 s.d.)
$1 - CL_s$ Observed	0.810 (0.88 s.d.)	0.878 (1.16 s.d.)	0.987 (2.23 s.d.)	0.990 (2.34 s.d.)

TABLE II: Expected and observed CL_{H_x} and $1 - CL_s$ values for $J^P = 0^-$ and $J^P = 2^+$ VX associated production, assuming signal cross sections equal to the 125 GeV SM Higgs production cross section multiplied by $\mu = 1.0$. The null hypothesis is taken to be the sum of the SM Higgs boson signal and background production.

Analysis	$ZH \rightarrow \ell\ell b\bar{b}$	$WH \rightarrow \ell\nu b\bar{b}$	$ZH \rightarrow \nu\nu b\bar{b}$	Combined
	$J^P = 0^-$ vs. $J^P = 0^+$			
CL_{0-} Expected	0.046	0.012	0.005	<0.0001
CL_{0-} Observed	0.072	0.245	0.0006	0.005
CL_{0+} Expected	0.500	0.500	0.500	0.500
CL_{0+} Observed	0.615	0.971	0.215	0.922
$1 - CL_s$ Expected	0.908 (1.33 s.d.)	0.975 (1.96 s.d.)	0.989 (2.31 s.d.)	0.9998 (3.60 s.d.)
$1 - CL_s$ Observed	0.883 (1.19 s.d.)	0.747 (0.67 s.d.)	0.997 (2.78 s.d.)	0.995 (2.56 s.d.)
	$J^P = 2^+$ vs. $J^P = 0^+$			
CL_{2+} Expected	0.037	0.003	0.009	<0.0001
CL_{2+} Observed	0.078	0.056	0.003	0.002
CL_{0+} Expected	0.500	0.500	0.500	0.500
CL_{0+} Observed	0.679	0.937	0.363	0.911
$1 - CL_s$ Expected	0.925 (1.44 s.d.)	0.995 (2.56 s.d.)	0.983 (2.11 s.d.)	0.9999 (3.86 s.d.)
$1 - CL_s$ Observed	0.885 (1.20 s.d.)	0.941 (1.56 s.d.)	0.991 (2.35 s.d.)	0.998 (2.91 s.d.)

TABLE III: Expected and observed CL_{H_x} and $1 - CL_s$ values for $J^P = 0^-$ and $J^P = 2^+$ VX associated production, assuming signal cross sections equal to the 125 GeV SM Higgs production cross section multiplied by $\mu = 1.23$. The null hypothesis is taken to be the sum of the SM Higgs boson signal and background production.

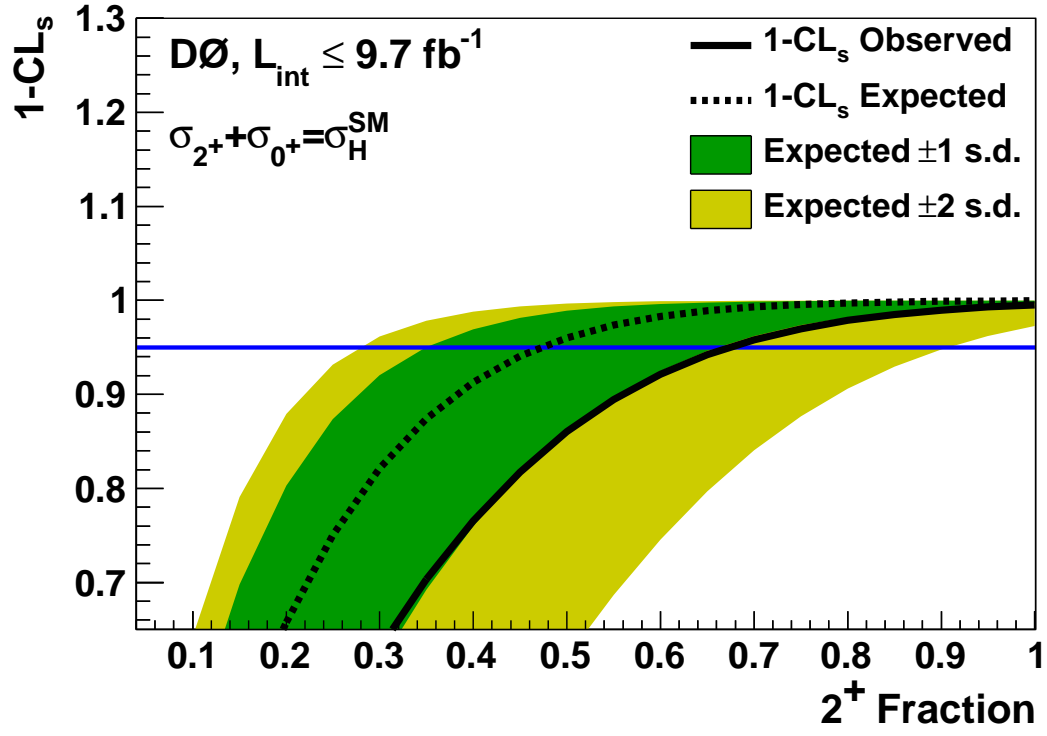


FIG. 12: (color online) $1 - CL_s$ as a function of the $J^P = 2^+$ signal fraction f_{2^+} for $\mu = 1.0$ for all analyses combined. The horizontal solid line corresponds to the 95% CL exclusion. The dark and light shaded regions represent the expected 1 and 2 s.d. fluctuations of the $J^P = 0^+$ hypothesis.

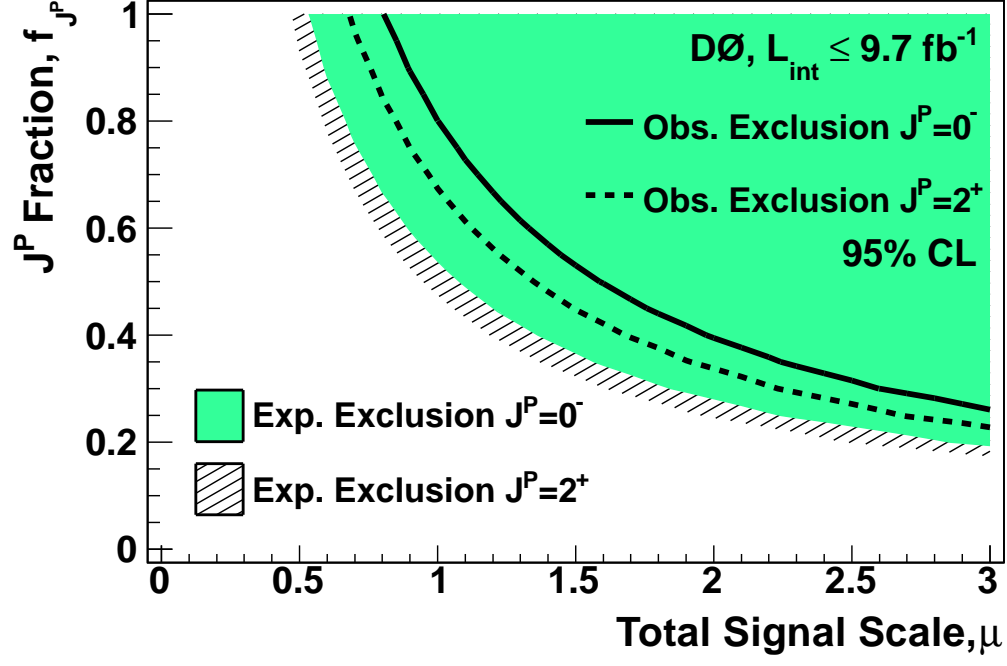


FIG. 13: (color online) The expected 95% CL exclusion (shaded area) and observed 95% CL exclusion (solid line) as functions of the $J^P = 0^-$ signal fraction f_{0^-} and the total signal strength in units of the SM Higgs cross section multiplied by the branching ratio. As functions of the $J^P = 2^+$ signal fraction f_{2^+} and the total signal strength, the expected and observed exclusions are shown as the hatched area and dashed line, respectively.